Dmitry D. Khalyavin*, Andrei N. Salak, Pascal Manuel, Nikolai M. Olekhnovich, Anatoly V. Pushkarev, Yury V. Radysh, Alexey V. Fedorchenko, Elena L. Fertman, Vladimir A. Desnenko and Mário G.S. Ferreira

Antisymmetric exchange in La-substituted $BiFe_{0.5}Sc_{0.5}O_3$ system: symmetry adapted distortion modes approach

DOI 10.1515/zkri-2015-1873
Received June 25, 2015; accepted August 21, 2015

Abstract: Neutron powder diffraction measurements on the 35 % La-substituted $Bi_{1-x}La_xFe_{0.5}Sc_{0.5}O_3$ composition revealed that the samples obtained under high-pressure (6 GPa) and high-temperature (1500 K) conditions crystalize into a distorted perovskite structure with the orthorhombic *Pnma* symmetry and the unit cell parameters: a_o = 5.6745(2) Å, b_o = 7.9834(3) Å and c_o = 5.6310(2) Å. A long-range magnetic ordering takes place below 220 K and implies a *G*-type magnetic structure with the moments 4.10(4)μ_B per Fe aligned predominately along the orthorhombic *c*-axis. The space group representation theory using the orthorhombic symmetry yields four bilinear coupling schemes for the magnetic order parameters imposed by antisymmetric exchange interactions. The couplings are analysed based on symmetry adapted distortion modes defined in respect of the undistorted cubic perovskite structure. The approach allows a quantitative estimation of the coupling strength. It is shown that the experimentally found spin configuration combines the magnetic order parameters coupled by the atomic displacement modes with the largest amplitudes. The results indicate that the antisymmetric exchange is the dominant anisotropic term which fully controls the direction of the Fe^{3+} spins in the distorted perovskite lattice.

Keywords: antisymmetric exchange; multiferroics; perovskites.

***Corresponding author: Dmitry D. Khalyavin,** ISIS Facility, Rutherford Appleton Laboratory OX11, 0QX Didcot, UK, E-mail: dmitry.khalyavin@stfc.ac.uk
Andrei N. Salak and Mário G.S. Ferreira: Department of Materials and Ceramic Engineering/CICECO, University of Aveiro, 3810-193 Aveiro, Portugal
Pascal Manuel: ISIS Facility, Rutherford Appleton Laboratory OX11, 0QX Didcot, UK
Nikolai M. Olekhnovich, Anatoly V. Pushkarev and Yury V. Radysh: Scientific-Practical Materials Research Centre of NAS of Belarus, P. Brovka, 19, 220072 Minsk, Belarus
Alexey V. Fedorchenko, Elena L. Fertman and Vladimir A. Desnenko: B. Verkin Institute for Low Temperature Physics and Engineering of NAS of Ukraine, Lenin Ave., 47, 61103 Kharkov, Ukraine

Introduction

A coupling between different order parameters is a general symmetry controlled phenomenon which is responsible for many useful physical properties of solids. Examples include piezoelectricity and piezomagnetism variety of optical and magnetoelectric effects. Cross-coupling between electronic and magnetic subsystems in multiferroic materials has attracted a particularly considerable attention in recent several years [1–3]. These materials combine spontaneous magnetic and electric dipole order parameters offering a unique opportunity of effective cross-control of their properties. In many type-II multiferroics, a spin-driven electric polarization is generated by inverse Dzyaloshinskii-Moria effect imposed by antisymmetric exchange interactions [1]. These interactions are also responsible for appearance of a weak ferromagnetism in some antiferromagnets including the important class of materials derived from the room-temperature type-I multiferroic $BiFeO_3$ [3]. In addition, antisymmetric exchange is a source of magnetic anisotropy in many magnetically-ordered compounds as well as it is the higher-order perturbation term which removes degeneracy and selects specific ordered states in some geometrically frustrated spin systems [4, 5].

Considering a pair of interacting spins, $\boldsymbol{S}_i$ and $\boldsymbol{S}_j$, whose local environments in a crystal are not related by inversion symmetry, the energy term representing the antisymmetric exchange is usually given by the mixed product $\boldsymbol{D}_{ij}[\boldsymbol{S}_i \times \boldsymbol{S}_j]$ (where the Dzyaloshinskii vector $\boldsymbol{D}_{ij}$ is a local characteristic of a given crystal). In the phenomenological description of the magnetic phase transition based

on the Landau theory, this energy term is mapped onto a bi-linear free-energy coupling invariant which is a simple product of two different magnetic order parameters with identical symmetry [6, 7]. A quantitative estimation of the coupling strength imposed by the antisymmetric exchange requires knowledge of the direction and value of the ***D***-vector for each exchange bond in the magnetic structure. In simple cases, when ***D*** is fixed by symmetry, the Moria rules and the Keffer formula can be the efficient tools [8, 9]. However, in a case of a low symmetry with complex structural distortions and exchange topology, analysis of antisymmetric exchange interactions is extremely difficult.

In the present work, we propose a simple symmetry based approach for a quantitative estimation of the coupling strength between different magnetic order parameters by means of antisymmetric exchange. This allows one to evaluate the contribution of the antisymmetric exchange to the magnetic anisotropy of the system, which dominates in many compounds containing 3*d* transition metals. The approach is based on the fact that the antisymmetric exchange is a coupling phenomenon imposed by structural distortions. The distortions can be decomposed into a set of symmetry-adapted displacement modes transformed by irreducible representations of undistorted parent structure [10–12]. A coupling between the magnetic order parameters is forbidden in this structure and therefore the structural distortions necessary for its appearance can be efficiently deduced. This can be done by working out free-energy coupling invariants which combine magnetic order parameters with the appropriate distortion modes. The amplitudes of these distortion modes, therefore, can be taken as the quantitative characteristic of the coupling.

We demonstrate the approach on a 35 % La-substituted $Bi_{1-x}La_xFe_{0.5}Sc_{0.5}O_3$. This is a particular composition studied as a part of our systematic research of multiferroic properties of the $Bi_{1-x}La_xFe_{1-y}Sc_yO_3$ perovskites obtained under extreme conditions [13, 14]. $Bi_{0.65}La_{0.35}Fe_{0.5}Sc_{0.5}O_3$ crystalizes into a distorted perovskite structure with orthorhombic *Pnma* symmetry and exhibits a long-range magnetic ordering below $T_N \sim 220$ K. The crystal and magnetic structures of the $Bi_{0.65}La_{0.35}Fe_{0.5}Sc_{0.5}O_3$ perovskite were fully characterized based on neutron diffraction data. The orthorhombic crystal structure involves several distortion modes providing a variety of coupling schemes for magnetic order parameters. We show that the experimentally found spin structure combines the magnetic order parameters coupled by the atomic displacement modes with the largest amplitudes.

Experimental section

High-purity oxides Bi_2O_3, La_2O_3, Fe_2O_3, and Sc_2O_3 were used as starting reagents. Previously calcined oxides were mixed in the stoichiometric ($Bi_{0.65}La_{0.35}Fe_{0.5}Sc_{0.5}O_3$) ratio, ball-milled in acetone, dried, and pressed into pellets. The pellets were heated in a closed alumina crucible at 1140 K for 10 min and then quenched down to room temperature. The obtained material served as a precursor for the high-pressure synthesis. The pressure was generated using an anvil press DO-138A with a press capacity up to 6300 kN. In order to avoid penetration of graphite from the tubular heater to the sample a protective screen of molybdenum foil was used. The samples were synthesized at 6 GPa and 1500 K. The high-pressure treatment time did not exceed 5 min.

An X-ray diffraction study of the powdered samples was performed using a PANalytical XPert MPD PRO diffractometer (Ni-filtered Cu K_α radiation, tube power 45 kV, 40 mA; PIXcell-1D detector, and the exposition corresponded to about 2 s per step of 0.02° over the angular range 15°–100°) at room temperature.

Neutron powder diffraction data were collected at the ISIS pulsed neutron and muon facility of the Rutherford Appleton Laboratory (UK), on the WISH diffractometer located at the second target station [15]. The sample (50 mg) was loaded into cylindrical 3 mm diameter vanadium can and measured in the temperature range of 1.5–300 K (step 30 K, exposition time 2 h) using an Oxford Instrument Cryostat. Rietveld refinements of the crystal and magnetic structures were performed using the FullProf program [16] against the data measured in detector banks at average 2θ values of 58°, 90°, 122°, and 154°, each covering 32° of the scattering plane. Group-theoretical calculations were done using ISOTROPY [17], ISODISTORT [10] and Bilbao Crystallographic Server (AMPLIMODES) [11, 12] software.

Magnetization data were measured using a superconducting quantum interference device (SQUID) magnetometer (Quantum Design MPMS).

Results and discussion

Crystal structure

The neutron diffraction pattern of $Bi_{0.65}La_{0.35}Fe_{0.5}Sc_{0.5}O_3$ collected at room temperature can be indexed using the orthorhombic *Pnma* space group and $\sqrt{2}a_p \times 2a_p \times \sqrt{2}a_p$ supercell (where a_p is the pseudocubic unit cell parameter), which implies the following relation between the orthorhombic and cubic cells:

$$\boldsymbol{a}_o = \boldsymbol{a}_p - \boldsymbol{c}_p, \quad \boldsymbol{b}_o = 2\boldsymbol{b}_p, \quad \boldsymbol{c}_o = \boldsymbol{a}_p + \boldsymbol{c}_p \tag{1}$$

A quantitative structure refinement indicates that the composition is isostructural to the distorted perovskites $LaFeO_3$ and $LaScO_3$. No structural phase transitions have been detected down to the lowest measured temperature 1.5 K. The refined structural parameters are listed in Table 1 and the fitting quality is illustrated in Figure 1a

Tab. 1: Atomic coordinates and thermal parameters (in Å^2) for $Bi_{0.65}La_{0.35}Fe_{0.5}Sc_{0.5}O_3$ at $T = 1.5$ K, refined in the *Pnma* space group with the basis vectors related to the parent cubic cell as $\boldsymbol{a}_o = \boldsymbol{a}_p - \boldsymbol{c}_p$, $\boldsymbol{b}_o = 2\boldsymbol{b}_p$, $\boldsymbol{c}_o = \boldsymbol{a}_p + \boldsymbol{c}_p$, and origin at (0, 0, 0).

Atom	Site	x	y	z	B_{iso}
Bi/La	4*c*	0.0221(6)	0.25	0.490(1)	1.98(7)
Fe/Sc	4*a*	0	0	0	1.62(5)
O1	4*c*	0.04820(9)	0.25	0.585(1)	1.7(2)
O2	8*d*	0.2910(5)	0.0456(5)	0.2136(1)	1.8(1)

Unit cell parameters: $a_o = 5.6745(2)$ Å, $b_o = 7.9834(3)$ Å and $c_o = 5.6310(2)$ Å.

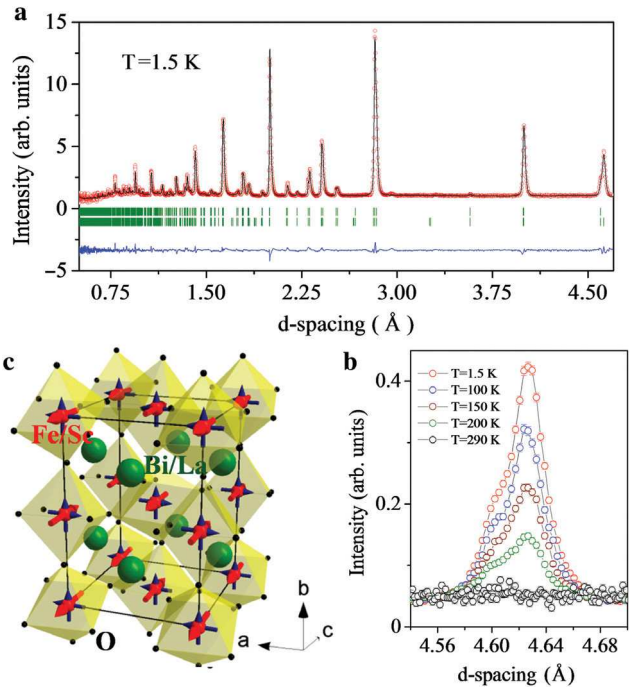

Fig. 1: (a) Rietveld refinement of the neutron diffraction data collected at 1.5 K ($R_{nucl} = 4.43$ %, $R_{mag} = 2.81$ %). The open symbols (red) and the solid line (black) represent the experimental and calculated intensities, respectively, and the line below (blue) is the difference between them. Tick marks (green) indicate the positions of Bragg peaks (*Pnma* space group): nuclear (top), and magnetic $\boldsymbol{k} = 0$ (bottom). (b) Neutron diffraction patterns at the vicinity of the strongest magnetic peaks collected at different temperatures. (c) Crystal and magnetic structures of $Bi_{0.65}La_{0.35}Fe_{0.5}Sc_{0.5}O_3$. The primary G_z and the secondary A_x/F_y modes are shown as red and blue arrows respectively.

for the highest resolution backscattering detectors bank. Although, the structural analysis did not reveal a significant polar/antipolar displacements of Bi and oxygen, like in the parent $BiFe_{0.5}Sc_{0.5}O_3$ composition [13], the large thermal parameters indicate a presence of static uncorrelated atomic displacements. The orthorhombic crystal structure involves a set of distortions which can be decomposed using the symmetry adapted displacement modes specified in terms of irreducible representations of the parent $Pm\bar{3}m$ space group. This mode decomposition procedure can be done automatically using either ISODISTORT [10] or AMPLIMODES [11, 12] software and the obtained result is summarized in Table 2. Two symmetry-adapted modes namely M_3^+ and R_4^+ related to oxygen displacements possess the largest amplitudes pointing to their primary character. These modes imply the in-phase and out-of-phase octahedral tilting, respectively, which are the general distortions in perovskite structures [18, 19]. The tilting scheme resulting in the orthorhombic *Pnma* ($\sqrt{2}a_p \times 2a_p \times \sqrt{2}a_p$) symmetry can be specified by the $a^-b^+a^-$ symbol using the Glazer's notations [18], which indicates that the pseudocubic $[010]_p$ and $[10\bar{1}]_p$ directions (or the *b* and *a*-axis in the orthorhombic setting (1)) are the tilting axis for the in-phase and out-of-phase octahedral rotations, respectively (see Figure 1c). This is

Tab. 2: Decomposition of the *Pnma* structure in respect of the symmetrized displacement modes of the parent cubic $Pm\bar{3}m$ perovskite structure ($a_p = 3.99528$ Å, Bi/La 1*b*(1/2, 1/2, 1/2), Fe/Sc 1*a*(0, 0,0) and O 3*d*(1/2, 0, 0)).

Irrep (*k*)	Order parameter	Site irrep	Amplitude
Strain			
$\Gamma_1^+(0, 0, 0)$	(δ), $e_{xx} + e_{yy} + e_{zz}$		0.00001
$\Gamma_3^+(0, 0, 0)$	$(\delta, -\sqrt{3}\delta)$, $-e_{xx} - e_{zz} + 2e_{yy}$		−0.00110
$\Gamma_3^+(0, 0, 0)$	$(0, 0, \delta)$, e_{xz}		−0.00544
Bi/La-displacement			
$R_5^+(1/2, 1/2, 1/2)$	$(r, r, 0)$	T_{1u}	−0.11300
$X_5^+(0, 1/2, 0)$	$(x, x, 0, 0, 0, 0)$	T_{1u}	0.24974
O-displacement			
$R_4^+(1/2, 1/2, 1/2)$	$(r, -r, 0)$	E_u	1.40794
$R_5^+(1/2, 1/2, 1/2)$	$(r, r\ 0)$	E_u	0.04954
$X_5^+(0, 1/2, 0)$	$(x, x, 0, 0, 0, 0)$	E_u	0.20341
$M_2^+(1/2, 0, 1/2)$	$(0, m, 0)$	A_{2u}	−0.05085
$M_3^+(1/2, 0, 1/2)$	$(0, m, 0)$	E_u	0.87578

The column "Irrep (*k*)" shows the irreducible representation of the $Pm\bar{3}m$ space group and the arms of the wave vector star involved. The column "Order parameter" lists the projections of the reducible order parameter onto the corresponding irreducible subspace (the same symbol in different positions indicates equal order parameter components). The columns "Site irrep" and "Amplitude" display the corresponding point-group symmetry irreps of the local Wyckoff position and the amplitudes (in Å) of the displacement modes, respectively. We use the standard supercell-normalized amplitudes defined as the square root of the sum of the squares of the mode-induced atomic displacements within the primitive supercell.

the most common tilting pattern observed in many other perovskite systems whose exceptional stability has been discussed by Woodward [20].

Magnetic structure

Magnetization measurements of $Bi_{0.65}La_{0.35}Fe_{0.5}Sc_{0.5}O_3$ revealed a weak ferromagnetic behaviour below $T_N \sim 220$ K (Figure 2) with the value of the spontaneous moment of ~0.16 emu/g. This value as well as the critical temperature of the magnetic ordering are very close to those observed in the antiferroelectric polymorph of $BiFe_{0.5}Sc_{0.5}O_3$ [13]. In agreement with the magnetization data, the neutron diffraction measurements indicate onset of a long-range antiferromagnetic ordering below T_N (Figure 1b). The observed magnetic reflections can be indexed using the $\sqrt{2}a_p \times 2a_p \times \sqrt{2}a_p$ orthorhombic cell pointing to the $\boldsymbol{k}_o = 0$ propagation vector. To refine quantitatively the magnetic structure, we classified the magnetic modes according to the time-odd irreducible representations of the *Pnma* space group [10, 17] and tested them in the refinement procedure. This approach based on the space groups representation theory developed by Bertaut [21] and Izumov [22] has been proven to be an efficient tool for the magnetic structures determination.

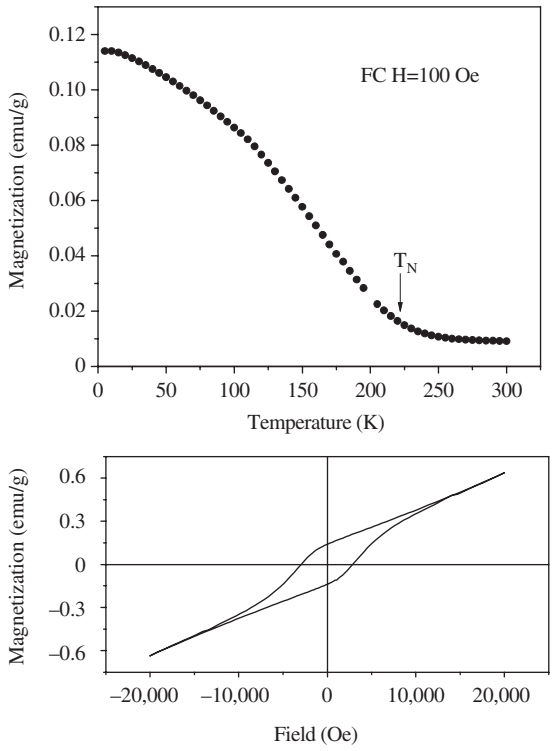

Fig. 2: Magnetization as a function of temperature, measured for $Bi_{0.65}La_{0.35}Fe_{0.5}Sc_{0.5}O_3$ under the magnetic field of H = 100 Oe after cooling in this field (top). Magnetization loop measured at 5 K after a zero-field cooling (bottom).

In the orthorhombic *Pnma* space group, the magnetic Fe^{3+} atoms occupy the $4a(0, 0, 0)$ Wyckoff position. The twelve-dimensional magnetic (pseudovector) reducible representation associated with this position is decomposed in terms of the irreducible representations of *Pnma* as:

$$\Gamma = 3m\Gamma_1^+ \oplus 3m\Gamma_2^+ \oplus 3m\Gamma_3^+ \oplus 3m\Gamma_4^+ \quad (2)$$

In order to emphasize the time-odd nature of the irreps, we use them with "*m*" letter following the ISODISTORT notations [10]. The decomposition indicates that the four one-dimensional parity-even irreps enter three times into the reducible representation, implying the existence of three orthogonal basis functions with identical symmetries for each irrep. Atomic components of these basis functions are given in Table 3 along with their widely used notations (A_i, C_i, G_i, F_i ($i = x, y, z$)) introduced by Bertaut [21]. The refinement procedure unambiguously yields the G_z mode (the moment size ~$4.10(4)\mu_B$ per Fe) with the symmetry of the $m\Gamma_4^+$ irrep as the primary irreducible magnetic order parameter. Presence of other two spin configurations, A_x and F_y transformed by the same irrep does not follow directly from the refinement, but they expected to be coupled to the G_z mode as secondary order parameters via a bi-linear free-energy invariant. This type of coupling is the "classic" case of a weak-ferromagnetism induced by the relativistic antisymmetric exchange [6–8]. The magnetization measurements (Figure 2) directly confirm the presence of an *F*-mode, in agreement with the symmetry arguments.

The primary *G*-type spin configuration found experimentally in $Bi_{0.65}La_{0.35}Fe_{0.5}Sc_{0.5}O_3$ suggests an antiferromagnetic orientation of spins in the nearest neighbour Fe/Sc sites. These spin correlations are naturally expected due to the strong 180-degree superexchange interactions caused by the half-occupied e_g orbitals of Fe^{3+}. These interactions are degenerate in respect of a global spin rotation and only higher order anisotropic terms in magnetic Hamiltonian can select between the G_x, G_y and G_z configurations. One of these anisotropic terms is antisymmetric exchange imposed by the structural distortions. In the next section we show that the experimentally found direction of the spins in the primary magnetic mode can be fully understood by considering the coupling with the secondary modes promoted by the antisymmetric Dzyaloshinskii–Moria interactions.

Tab. 3: Atomic components of the pseudovector basis functions localized on the 4*a* Wyckoff position for the time-odd irreducible representations of the *Pnma* space group associated with the $\boldsymbol{k}_o = 0$ propagation vector.

Irrep	$m\Gamma_1^+$	$m\Gamma_1^+$	$m\Gamma_1^+$	$m\Gamma_2^+$	$m\Gamma_2^+$	$m\Gamma_2^+$	$m\Gamma_3^+$	$m\Gamma_3^+$	$m\Gamma_3^+$	$m\Gamma_4^+$	$m\Gamma_4^+$	$m\Gamma_4^+$
Mode	G_x	C_y	A_z	C_x	G_y	F_z	F_x	A_y	C_z	A_x	F_y	G_z
Atom												
(0, 0, 0)	1	0	0	1	0	0	1	0	0	1	0	0
	0	1	0	0	1	0	0	1	0	0	1	0
	0	0	1	0	0	1	0	0	1	0	0	1
(1/2, 1/2, 1/2)	1	0	0	−1	0	0	1	0	0	−1	0	0
	0	−1	0	0	1	0	0	−1	0	0	1	0
	0	0	−1	0	0	1	0	0	−1	0	0	1
(0, 1/2, 0)	−1	0	0	1	0	0	1	0	0	−1	0	0
	0	1	0	0	−1	0	0	−1	0	0	1	0
	0	0	−1	0	0	1	0	0	1	0	0	−1
(1/2, 0, 1/2)	−1	0	0	−1	0	0	1	0	0	1	0	0
	0	−1	0	0	−1	0	0	1	0	0	1	0
	0	0	1	0	0	1	0	0	−1	0	0	−1

Coupling of magnetic modes

The symmetry analysis based on the orthorhombic *Pnma* space group discussed in the previous section yields bilinear coupling schemes for the magnetic order parameters transformed by the same irreps. This approach, however, does not tell anything about the strength of the coupling and therefore is not able to distinguish which of the three configurations G_x, G_y and G_z is preferable in respect of the antisymmetric exchange. The issue can be resolved, if one considers the coupling terms written down in respect of the cubic $Pm\bar{3}m$ space group. This symmetry describes undistorted perovskite structure where the magnetic modes specified in Table 3 are transformed by different irreps and specific structural distortions are required to combine them into a free-energy coupling terms (invariant in respect of the cubic symmetry). The structural distortions providing the coupling are the key ingredient of the approach. We are particularly interested in the distortions involving displacements of oxygen since the superexchange between Fe^{3+} spins is mediated by these ions. The decomposition of the orthorhombic crystal structure in terms of the symmetry adapted basis of the $Pm\bar{3}m$ space group described in the section "Crystal structure" provides the numerical amplitudes for each distortion mode. These amplitudes can be taken as the quantitative characteristic of the couplings.

Let us analyse the free-energy coupling terms activated by the G_x, G_y and G_z spin configurations using the approach discussed above. As a first step, we need to define the magnetic modes specified in Table 3 in terms of the irreducible representations of the cubic $Pm\bar{3}m$ space group. This can be done by generating basis functions localized on the Fe/Sc sites for different irreps of the cubic space group, or simpler by using the algorithms of magnetic modes decomposition, implemented into the ISODISTORT software [10]. Table 4 shows the relevant irreps and the order parameter directions for each magnetic mode. Below, we discuss separately the coupling schemes for the different spin configurations.

(i) The spin components in the primary *G*-type magnetic mode are along the orthorhombic *a*-axis (G_x-mode).

Tab. 4: Magnetic modes of the orthorhombic *Pnma* space group expressed in terms of the irreducible representations of the cubic $Pm\bar{3}m$ symmetry.

***Pnma* Irrep**	**Mode**	***Pm*$\bar{3}$*m* irrep (*k*)**	**Order parameter**
$m\Gamma_1^+$	G_x	$mR_4^+(1/2, 1/2, 1/2)$	$(g, -g, 0)$
	C_y	$mM_3^+(1/2, 0, 1/2)$	$(0, c, 0)$
	A_z	$mX_5^+(0, 1/2, 0)$	$(a, a, 0, 0, 0, 0)$
$m\Gamma_2^+$	C_x	$mM_5^+(1/2, 0, 1/2)$	$(0, 0, c, -c, 0, 0)$
	G_y	$mR_4^+(1/2, 1/2, 1/2)$	$(0, 0, g)$
	F_z	$m\Gamma_4^+(0, 0, 0)$	$(f, 0, f)$
$m\Gamma_3^+$	F_x	$m\Gamma_4^+(0, 0, 0)$	$(f, 0, -f)$
	A_y	$mX_3^+(0, 1/2, 0)$	$(a, 0, 0)$
	C_z	$mM_5^+(1/2, 0, 1/2)$	$(0, 0, c, c, 0, 0)$
$m\Gamma_4^+$	A_x	$mX_5^+(0, 1/2, 0)$	$(a, -a, 0, 0, 0, 0)$
	F_y	$m\Gamma_4^+(0, 0, 0)$	$(0, f, 0)$
	G_z	$mR_4^+(1/2, 1/2, 1/2)$	$(g, g, 0)$

The C_y and A_z spin configurations are transformed by the same one-dimensional $m\Gamma_1^+$ irrep of the *Pnma* space group (see Table 3) implying that the products G_xC_y and G_xA_z are invariants in respect of this symmetry. These magnetic modes, however, are transformed by different irreps of the cubic $Pm\bar{3}m$ space group (Table 4) and therefore, the lowest degree coupling terms invariant in respect of this symmetry can only be trilinear. Using the ISOTROPY software [17], one can find out that the products respecting all the symmetry operations of $Pm\bar{3}m$, including the time-reversal and translational symmetries, are:

$$x_1g_2c_2 - x_2g_1c_2 + x_3g_1c_3 - x_4g_3c_3 + x_5g_3c_1 - x_6g_2c_1 \quad (3)$$

$$m_1g_2a_6 - m_1g_3a_5 + m_2g_1a_2 - m_2g_2a_1 - m_3g_1a_3 + m_3g_3a_4 \quad (4)$$

where $x_i(i = 1–6)$, $g_i(i = 1–3)$, $c_i(i = 1–3)$, $m_i(i = 1–3)$ and $a_i(i = 1–6)$ are components of the X_5^+, mR_4^+, mM_3^+, M_3^+, and mX_5^+ order parameters, respectively. These general invariants (written down for the general directions of the corresponding order parameters, when all the components are non-zero and different) are reduced down to $-x_1gc–x_2gc$ and $m_2ga + m_2ga$ for the $mR_4^+(g, -g, 0) \equiv G_x$, $mM_3^+(0, c, 0) \equiv C_y$ and the $mR_4^+(g, -g, 0) \equiv G_x$, $mX_5^+(a, a, 0, 0, 0, 0) \equiv A_z$ order parameters, respectively. Thus, the coupling between the G_x and C_y spin configurations is imposed by the $X_5^+(x_1, x_2, 0, 0, 0, 0) = (x, x, 0, 0, 0, 0;$ at $x_1 = x_2 = x)$ structural distortion (free-energy term $-2xgc$), whereas the coupling between G_x and A_z is proportional to the amplitude of the $M_3^+(0, m_2 = m, 0)$ distortive mode (free-energy term $2mga$). This result is illustrated in Figure 3, where the oxygen displacements in the $X_5^+(x, x, 0, 0, 0, 0)$ and $M_3^+(0, m, 0)$ are shown along with the magnetic modes coupled by these structural distortions.

(ii) The spin components in the primary *G*-type magnetic mode are along the orthorhombic *y*-axis (G_y-mode). In this case, the antisymmetric exchange interactions couple the C_x and F_z secondary magnetic order parameters transformed by the $m\Gamma_2^+$ irrep of *Pnma* (Table 3). The general free-energy coupling terms invariant under symmetry operations of the cubic $Pm\bar{3}m$ space group [17] are:

$$x_1g_3c_4 - x_2g_3c_3 + x_3g_2c_6 - x_4g_2c_5 + x_5g_1c_2 - x_6g_1c_1 \quad (5)$$

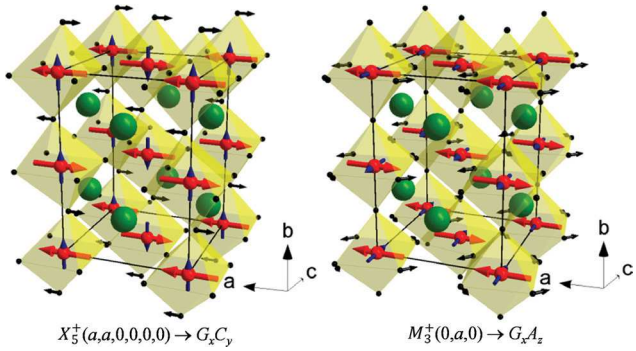

Fig. 3: $X_5^+(a, a, 0, 0, 0, 0)$ displacement mode (black arrows on the oxygen ions) coupling the G_x (red arrows on the Fe/Sc ions) and C_y (blue arrows on the Fe/Sc ions) magnetic order parameters (left). $M_3^+(0, m, 0)$ displacement mode (black arrows on the oxygen ions) coupling the G_x (red arrows on the Fe/Sc ions) and A_z (blue arrows on the Fe/Sc ions) magnetic order parameters (right).

$$r_1g_2f_2 - r_1g_3f_1 - r_2g_1f_2 + r_2g_3f_3 + r_3g_1f_1 - r_3g_2f_3 \quad (6)$$

where $x_i(i = 1–6)$, $g_i(i = 1–3)$, $c_i(i = 1–6)$, $r_i(i = 1–3)$ and $f_i(i = 1–3)$ are components of the X_5^+, mR_4^+, mM_5^+, R_4^+, and $m\Gamma_4^+$ order parameters, respectively. They are reduced down to $-x_1gc - x_2gc$ and $-r_1gf + r_2gf$ for the $mR_4^+(0, 0, g) \equiv G_y$, $mM_5^+(0, 0, c, -c, 0, 0) \equiv C_x$ and $mR_4^+(0, 0, g) \equiv G_y$, $m\Gamma_4^+(f, 0, f) \equiv F_z$ order parameters, respectively. These implies that the C_x and F_z spin configurations are coupled to the G_y magnetic mode by the $X_5^+(x_1, x_2, 0, 0, 0, 0) = (x, x, 0, 0, 0, 0;$ at $x_1 = x_2 = x)$ and $R_4^+(-r_1, r_2, 0) = (r, -r, 0;$ at $-r_1 = r_2 = r)$ structural distortions, respectively as illustrated in Figure 4. The

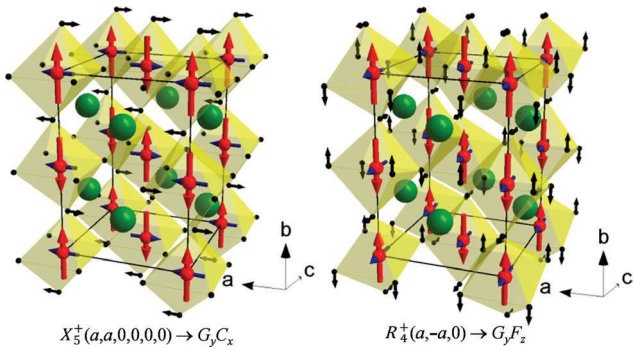

Fig. 4: $X_5^+(a, a, 0, 0, 0, 0)$ displacement mode (black arrows on the oxygen ions) coupling the G_y (red arrows on the Fe/Sc ions) and C_x (blue arrows on the Fe/Sc ions) magnetic order parameters (left). $R_4^+(r, -r, 0)$ displacement mode (black arrows on the oxygen ions) coupling the G_y (red arrows on the Fe/Sc ions) and F_z (blue arrows on the Fe/Sc ions) magnetic order parameters (right).

corresponding non-vanishing free-energy coupling terms are $-2xgc$ and $2rgf$.

(iii) The spin components in the primary G-type magnetic mode are along the orthorhombic z-axis (G_z-mode transformed by the Γ_4^+ irrep of $Pnma$). The structural distortions which couple the A_x and F_y secondary magnetic order parameters to the primary one G_z are defined by the general free-energy terms (4) and (6) and by the corresponding order parameters directions in the representation spaces of the cubic $Pm\bar{3}m$ space group (Table 4). The G_z and A_x spin configurations are specified by the $mR_4^+(g, g, 0)$ and $mX_5^+(a, -a, 0, 0, 0, 0)$ irreps, respectively, which reduce the general term (4) down to $-m_2ga - m_2ga$. The latter shows that the coupling is activated by the $M_3^+(0, m_2 = m, 0)$ structural distortion. Analogously, $mR_4^+(g, g, 0)$ and $\Gamma_4^+(0, f, 0)$ reduce the coupling term (6) down to $r_1gf - r_2gf$, indicating that the coupling is imposed by the $R_4^+(r_1, -r_2, 0) = (r, -r, 0;$ at $r_1 = -r_2 = r)$ structural distortion (see Figure 5).

Then, by comparing the amplitudes for the structural distortion modes listed in Table 1, one can conclude that the G_z spin configuration allows to activate the coupling terms imposed by the largest structural distortions, namely by the in-phase and out-of-phase octahedral tilting. As shown above, this spin configuration has indeed been found experimentally. This result indicates that the antisymmetric exchange is the dominant anisotropic interaction which controls the direction of the Fe^{3+} spins in the primary G-type spin configuration.

It should be pointed out that the role of octahedral tilting in coupling of magnetic modes in perovskites has also been highlighted by Bellaiche, Gui and Kornev [23]. The authors formulated an elegant coupling law (see equation 4 of Ref. [23]) relating the in-phase and out-of-phase octahedral tilting with the A, C, G and F, spin configurations. The results obtained here based on the symmetry arguments are fully consistent with this expression. Our approach is however much more general and is not restricted by the case of the octahedral tilting in perovskites only. It provides a way to quantify the magnetic coupling in different structures with any types of distortions, including incommensurate ones as we recently showed [24], and can be adopted to analyse a wide range of problems.

Finally, let us briefly discuss some limitations and further possible improvements of the symmetry based approach presented above. The simple example used in the present work demonstrates only the basic ideas how the symmetry methods can be used to evaluate coupling between magnetic order parameters and its impact on the magnetic structure. The studied perovskite compound contains octahedrally coordinated Fe^{3+} ions with the $e_g^2t_{2g}^3$ electronic configuration which implies a nearly quenched orbital momentum (L = 0, S = 5/2) and therefore no significant single ion anisotropy effects. In some other materials, with different electronic configurations of transition metals imposed by their charge state, coordination and crystal fields, the single ion anisotropy can be significant and can compete with antisymmetric exchange, making the prediction of the spin direction based on the symmetry arguments only, to be difficult.

Another limitation comes from the fact that the procedure can be applied only if the magnetic atoms occupy a single Wyckoff position in the parent structure (in respect of which the mode decomposition is done). Evaluation of the coupling arising from interactions between non-symmetry related sites in the parent structure cannot be done based on the symmetry consideration.

The corner-sharing network of the $Fe^{3+}O_6$ octahedra in the perovskite structure of $Bi_{0.65}La_{0.35}Fe_{0.5}Sc_{0.5}O_3$ also implies (at least to a first approximation) an isotropic exchange interactions. In some other materials, with low-dimensional crystal structures or orbital ordering, the exchange topology can be strongly anisotropic and this fact must be taken into account. This can be done by introducing additional weighting factors to the standard definition of the mode amplitude, which depend on the number of 'strong' and 'weak' bonds (in respect of the symmetric exchange) affected by the particular displacement mode. In these cases, knowledge of the exchange parameters from independent measurements or calculations is crucial. Even in the case of an isotropic exchange

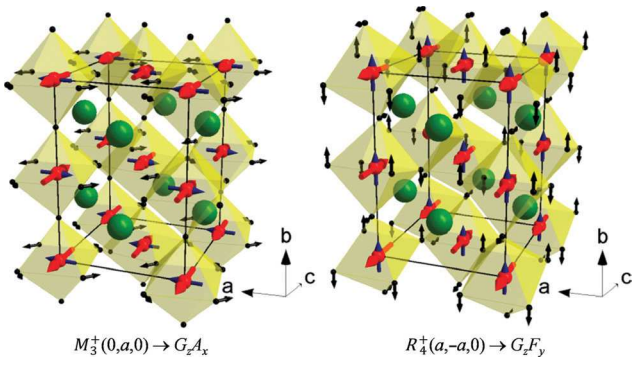

Fig. 5: $M_3^+(0, m, 0)$ displacement mode (black arrows on the oxygen ions) coupling the G_z (red arrows on the Fe/Sc ions) and A_x (blue arrows on the Fe/Sc ions) magnetic order parameters (left). $R_4^+(r, -r, 0)$ displacement mode (black arrows on the oxygen ions) coupling the G_z (red arrows on the Fe/Sc ions) and F_y (blue arrows on the Fe/Sc ions) magnetic order parameters (right).

topology, the coupling strength depends on the number of exchange bonds affected by atomic displacements in a specific distortive mode. For instance, the X_5^+ mode in Figure 3 (left) distorts only two out of the six nearest neighbour Fe-O-Fe superexchange bonds, while the M_3^+ mode [Figure 3 (right)] affects four superexchange paths. Thus, at equal absolute displacements of oxygen ions in the X_5^+ and M_3^+ modes, the latter will provide a twice bigger energy gain from the antisymmetric exchange at the appropriate direction of the moments in the primary *G*-type spin configuration. In principle, the standard definition of the supercell-normalized amplitude (the square root of the sum of the squares of the mode-induced atomic displacements) takes into account the number of displaced atoms but not the number of the affected exchange bonds and their strength. In some cases, therefore, it would be more appropriate to use absolute atomic displacements which can be easily obtained from the multi-atom mode vectors and the corresponding normalizing factors provided by the ISODISTORT and AMPLIMODES software [10–12]. These absolute atomic displacements combined with the normalization to the number of the affected exchange bonds and their strength can provide a better evaluation of the magnetic coupling imposed by these distortions.

Conclusions

The $Bi_{0.65}La_{0.35}Fe_{0.5}Sc_{0.5}O_3$ composition obtained under high-pressure and high-temperature conditions crystalizes into distorted perovskite structure with the orthorhombic *Pnma* ($\sqrt{2}a_p \times 2a_p \times \sqrt{2}a_p$) symmetry. The largest structural distortions involve the in-phase and out-of-phase octahedral tilting with the $a^-b^+ - a^-$ tilting pattern. The long-range antiferromagnetic ordering with the primary G_z spin configuration occurs below $T_N \sim 220$ K. This magnetic order parameter couples two secondary magnetic modes A_x and F_y via antisymmetric exchange interactions imposed by the in-phase and out-of-phase octahedral tilting, respectively. The direction of the Fe^{3+} spins in the primary *G*-type spin configuration is fully controlled by the antisymmetric exchange which is the dominant anisotropic interaction in the system.

Acknowledgments: This work was supported by project TUMOCS. This project has received funding from the European Union's Horizon 2020 research and innovation programme under the Marie Skłodowska-Curie grant agreement No 645660.

References

[1] S.-W. Cheong, M. Mostovoy, *Nat. Mater.* **2007**, *6*, 13.
[2] G. Catalan, J. F. Scott, *Adv. Mater.* **2009**, *21*, 2463.
[3] A. P. Pyatakov, A. K. Zvezdin, *Physics – Uspekhi* **2012**, *55*, 557.
[4] M. Elhajal, B. Canals, C. Lacroix, *Phys. Rev. B* **2002**, *66*, 014422.
[5] L. Messio, O. Cepas, C. Lhuillier, *Phys. Rev. B* **2010**, *81*, 064428.
[6] I. E. Dzialoshinskii, *Sov. Phys. JETP* **1957**, *5*, 1259.
[7] I. Dzyaloshinskii, *J. Phys. Chem. Solids* **1958**, *4*, 241.
[8] T. Moriya, *Phys. Rev.* **1960**, *120*, 91.
[9] F. Keffer, T. Moriya, *Phys. Rev.* **1962**, *126*, 896.
[10] B. J. Campbell, H. T. Stokes, D. E. Tanner, D. M. Hatch, *J. Appl. Crystallogr.* **2006**, *39*, 607.
[11] D. Orobengoa, C. Capillas, M. I. Aroyo, J. M. Perez-Mato, *J. Appl. Cryst.* **2009**, *42*, 820.
[12] J. M. Perez-Mato, D. Orobengoa, M. I. Aroyo, *Acta Cryst A* **2010**, *66*, 558.
[13] D. D. Khalyavin, A. N. Salak, N. M. Olekhnovich, A. V. Pushkarev, Yu. V. Radyush, P. Manuel, I. P. Raevski, M. L. Zheludkevich, M. G. S. Ferreira, *Phys. Rev. B* **2014**, *89*, 174414.
[14] S. A. Prosandeev, D. D. Khalyavin, I. P. Raevski, A. N. Salak, N. M. Olekhnovich, A. V. Pushkarev, Yu V. Radyush, *Phys. Rev. B* **2014**, *90*, 054110.
[15] L. C. Chapon, P. Manuel, P. G. Radaelli, C. Benson, L. Perrott, S. Ansell, N. J. Rhodes, D. Raspino, D. Duxbury, E. Spill, J. Norris, *Neutron News* **2011**, *22*, 22.
[16] J. Rodriguez Carvajal, *Physica B* **1993**, *193*, 55.
[17] H. T. Stokes, D. M. Hatch, B. J. Campbell, ISOTROPY Software Suite, iso.byu.edu.
[18] A. M. Glazer, *Acta Crystallogr. B* **1972**, *28*, 3384.
[19] C. J. Howard, H. T. Stokes, *Acta Crystallogr.* **1998**, *B54*, 782.
[20] P. M. Woodward, *Acta Cryst. B* **1997**, *53*, 44.
[21] E. F. Bertaut, *Acta Cryst. A* **1968**, *24*, 217.
[22] Yu. A. Izumov, V. E. Naish, R. P. Ozerov, *Neutron Diffraction of Magnetic Materials*, Consulting Bureau, New York, **1991**.
[23] L. Bellaiche, Z. Gui, I. A. Kornev, *J. Phys.: Condens. Matter* **2012**, *24*, 312201.
[24] D. D. Khalyavin, A. N. Salak, A. B. Lopes, N. M. Olekhnovich, A. V. Pushkarev, Yu. V. Radyush, E. L. Fertman, V. A. Desnenko, A. V. Fedorchenko, P. Manuel, A. Feher, J. M. Vieira, M. G. S. Ferreira, arXiv:1508.07915.

Graphical Synopsis

Dmitry D. Khalyavin, Andrei N. Salak, Pascal Manuel, Nikolai M. Olekhnovich, Anatoly V. Pushkarev, Yury V. Radysh, Alexey V. Fedorchenko, Elena L. Fertman, Vladimir A. Desnenko and Mário G.S. Ferreira

Antisymmetric exchange in La-substituted $BiFe_{0.5}Sc_{0.5}O_3$ system: symmetry adapted distortion modes approach

DOI 10.1515/zkri-2015-1873
Z. Kristallogr. 2015; x: xxx–xxx

Synopsis: Based on symmetry adapted distortion modes approach, a method to evaluate a coupling between magnetic order parameters imposed by antisymmetric exchange has been proposed.